Journal of Theoretical and Applied Mechanics, Sofia, Vol. 47 No. 3 (2017) pp. 59-80
FLUID MECHANICS

FAILURE MECHANISMS OF BRITTLE ROCKS UNDER UNIAXIAL COMPRESSION

TAOYING LIU[1,2*], PING CAO[1]

[1]*School of Resources & Safety Engineering, Central South University, Changsha, Hunan, 410083, China*
[2]*Ma'anshan Institute of Mining Research, Ma'anshan, Anhui, 243004, China*

[Received 09 August 2016. Accepted 26 June 2017]

ABSTRACT: The behaviour of a rock mass is determined not only by the properties of the rock matrix, but mostly by the presence and properties of discontinuities or fractures within the mass. The compression test on rock-like specimens with two prefabricated transfixion fissures, made by pulling out the embedded metal inserts in the pre-cured period was carried out on the servo control uniaxial loading tester. The influence of the geometry of pre-existing cracks on the cracking processes was analysed with reference to the experimental observation of crack initiation and propagation from pre-existing flaws. Based on the rock fracture mechanics and the stress-strain curves, the evolution failure mechanism of the fissure body was also analyzed on the basis of exploring the law of the compression-shear crack initiation, wing crack growth and rock bridge connection. Meanwhile, damage fracture mechanical models of a compression-shear rock mass are established when the rock bridge axial transfixion failure, tension-shear combined failure, or wing crack shear connection failure occurs on the specimen under axial compression. This research was of significance in studying the failure mechanism of fractured rock mass.

KEY WORDS: Brittle rocks, crack coalescence mechanism, wing crack, rock fracture mechanics, uniaxial compression.

LIST OF SYMBOLS

σ	uniaxial compression (MPa);	ψ	angle between σ and the crack face;
θ	cracking angle of wing crack;	α	inclination angle of rock bridge;
β	inclination angle of main crack;	b	rock bridgelength;
σ_{ne}, τ_{ne}	normal and shear stress on crack plane (MPa);	K_I	mode I stress intensity factor (MPa m$^{1/2}$);
K_{II}	mode II stress intensity factor (MPa m$^{1/2}$);	K_{IC}	mode I fracture toughness (MPa m$^{1/2}$);
l	extension of wing crack (m);	$2a$	length of initial, angled crack (m);
l_{ty}	influence coefficient;	L,	equivalent crack length ($L = l/a$);
		c	cohesion

*Corresponding author e-mail: liutaoying_csu@163.com

1. INTRODUCTION

Rock material is typically inhomogeneous, containing defects such as joints, faults and micro cracks or other defects. The existence of discontinuities in the rock usually has two effects (Bobet 1997 [4]; Dyskin et al 2003 [7]; Park and Bobet 2010 [14]): (1) they decrease the strength and stiffness of the rock; and (2) they are a source of initiation of new discontinuities, which in turn may propagate and link with other cracks and further decrease the strength and the stiffness of the rock, which is significant to predict unstable failure properties of jointed rock mass engineering. Meanwhile, the crack initiation from micro-cracks progressing to a completely damaged rock mass is a process of evolution and an accumulation of rock mass damage from fractures connecting existing cracks. Rock bridge fracture among multi-crack is one of the important reasons for rock mass failure. If the crack distribution near a rock bridge is known, it is the prerequisite to predict or refrain the failure of this kind of rock mass that the patterns, mechanism of failure and loading conditions are foreknown.

The extension of cracks depends on the properties of cracks such as size, location, orientation and loading condition, a thorough understanding of the cracking processes, emanating from exiting flaws, will benefit geological engineering design and implementation, including rock slope or foundation stability analysis, tunnel support design, and fluid flow prediction in rock masses. Due to the difficulties of using authentic rock materials in-situ tests, the laboratory loading test of rock-like materials was an effective research method and used widely. A vast number of scholars have made great effort to developing crack propagation theories (Kemeny and Cook 1987 [10]; Lajtai 1998 [12]; Hoekand Martin 2014 [8]; Cao et al 2015 [5]) or developing techniques to study coalescence process of cracks, existed in a rock mass under external loads (Tang and Kou 1998 [17]; Wong and Einstein 2009 [19]; Zhang and Wong 2013 [22]), or studying the relationship between micro damage development and macro deformation of rock under uniaxial compression (Kemeny 1991 [11]; Zhou and Zhang 2008 [24]; Yang et al 2012 [21]). Especially with the use of the high speed video technology, scanning electron microscopy (SEM) and computed tomography (CT) scan technique, the progressive failure mechanisms have been observed in detail. Similarly, various numerical studies using different techniques have been successfully used in modelling such progressive failure mechanism. Significant advances have been made in understanding the failure process of brittle rock. It is currently recognized that damage initiates primarily in the form of extensile microcracks, that originate from local stress concentrations. The mechanism of frictional sliding on pre-existing cracks is generally recognized as the primary stress concentrator, that produces wing crack growth under the compressive stress field. Meanwhile, by introducing rock fracture mechanics, it is possible to provide a fundamental basis in researching crack propagation and coalescence mechanism.

In this paper, the compression test on rock-like specimens with two prefabricated transfixion fissures, made by pulling out the embedded metal inserts in the pre-cured period was performed on the servo control uniaxial loading tester. The influences of the geometry of pre-existing cracks on the failure processes were analyzed with reference to the experimental observation of crack initiation and propagation from pre-existing flaws in rock specimens in compression. Based on previous studies and the rock fracture mechanics criterion, this paper proposes mechanical models of the failure rock mass. Then combined with the stress-strain curves, the gradual fracture and damage evolution of the rock mass was studied on the basis of exploring the law of the compression-shear crack initiation, wing crack growth and rock bridge connection. This paper is an attempt at studying the failure model and crack coalescence mechanism of brittle rocks under uniaxial compression. The results obtained were of significance in studying the failure mechanism of fractured rock mass.

2. LABORATORY EXPERIMENT OF BRITTLE ROCK

Cement mortar specimens were used in this study, based on the similar mechanical properties with natural rock masses. The rock-like materials were composited of a mixture of water, white cement, and silica sand. The external measurement of specimens was 200 mm $\times$ 150 mm $\times$ 30 mm, and the prefabricated transfixion fissures were made by pulling out an embedded metal inserts (0.4 mm thickness) in the pre-cured period; and the length of fissures was 20 mm. The two flaws are located at the center of the specimen and the inclination measured from horizontal are separately: $\beta = 25°$, $\beta = 45°$, $\beta = 60°$, $\beta = 75°$, and the inclination angle of rock bridge α are separately: $\alpha = 25°$, $\alpha = 45°$, $\alpha = 60°$, $\alpha = 75°$, where $\alpha \geq \beta$, b is the rock bridge with a length of 40 mm, the details of specimens are shown in Fig. 1.

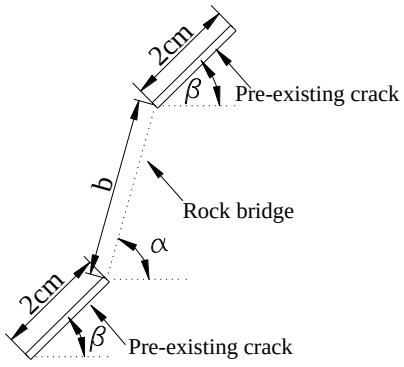

Fig. 1. Physical test specimen.

Fig. 2. Electro-hydraulic servo control testing machine.

Combined with the loading control system DCS-200, this testing was carried out on the servo control uniaxial loading instrument, as shown in Fig. 2. The loading rate was set to be 50 N/s. In order to reduce the influence of the end effect, two rubber cushions, coated with butter, were placed between the ends of the specimen and pressure plates of the instrument. During the loading process, failure patterns and stress-strain curves of specimens were observed and recorded by camera, and the clock gauge set on the middle part of side was used to indicate the transverse deformation behaviours of specimens.

Meanwhile, taking the complete rock specimens for testing, the stress strain curve of the intact specimen is shown in Fig. 3, and the physical and mechanical parameters of this rock specimen are obtained, as is shown in Table 1.

Table 1. Mechanical parameters of rock-like materials under uniaxial compression

Density g/cm^3	Modulus of elastic MPa	Uniaxial compressive strength MPa	Uniaxial tensile strength MPa	Poisson's ratio
2.019	2.272e3	22.52	2.75	0.2251

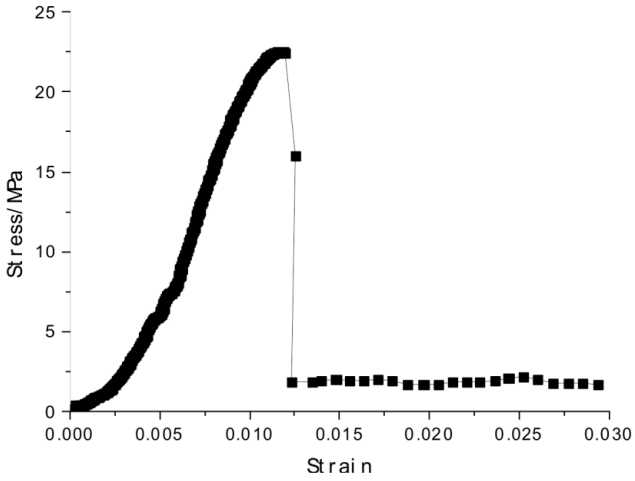

Fig. 3. The stress strain curve of the intact specimen.

3. WING CRACK INITIATION AND PROPAGATION

3.1. CRACK INITIATION

The underground rock usually exists in a compression stress state, and a lot of testing results and theoretical calculation prove that cracks expand approximately in the direction parallel to the maximum principal stress under the action of stress (Ashby and Hallam 1986 [1]; Cao and Pu 2012 [6]), as shown in Fig. 4.

Firstly, this paper assumes the rock mass is categorized as crisp flexible, meet

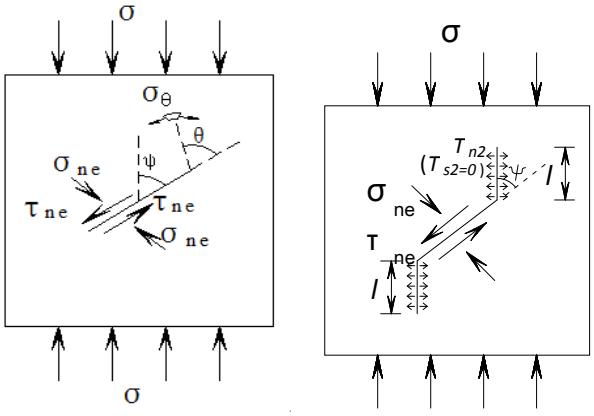

Fig. 4. Sketch of wing cracks seeding and propagation.

the theory of linear-elastic fracture mechanics. The fractured rock mass is under uniaxial compression σ, and the angle between the crack face and vertical stress σ is ψ. Based on the theory of materials mechanics, the normal stress σ_{ne} and the shear driving force τ_{ne} appear in following formulas (Li 1999 [13]) (Here the compressive stress is positive).

$$\sigma_{ne} = \sigma \sin^2 \psi \,, \tag{1}$$

$$\tau_{ne} = \sigma \sin \psi \cos \psi \,. \tag{2}$$

To establish the crack tip, as the origin in the polar coordinates system (r, θ), σ_θ, can be expressed as (Zheng 2000 [23]):

$$\sigma_\theta = \frac{3}{2} \frac{\tau_{_{eff}} \sqrt{\pi a}}{\sqrt{2\pi r}} \sin\theta \cos\frac{\theta}{2} \,. \tag{3}$$

According to the maximum circumferential stress criterion, the initial crack extends along the direction of the maximum normal stress. Thus, the cracking angle $\theta = 70.5$ can be obtained from (Ashby and Sammis1990 [2]):

$$\frac{\partial \sigma_\theta}{\partial \theta} = 0 \,. \tag{4}$$

Then, the stress intensity factor at the wing crack initiation can be concluded as (Zheng 2000 [23]):

$$K_I = \frac{2}{\sqrt{3}} \tau_{ne} \sqrt{\pi a} \,. \tag{5}$$

When $K_I = K_{IC}$ in Eq. (3), the rock began to crack, where K_{IC} is the fracture toughness.

3.2. WING CRACK PROPAGATION

A lot of engineering cases and experiment results show that rock ruptures owing to cracks propagation, growth and integration. Many researches show, that cracks kink to the mode-I fracture under compressive-shear stresses state. When $K_I > K_{IC}$, wing crack initiates then propagates at the tip of the main crack and the stress intensity factor of wing crack varies with the propagation of wing crack. Based on fracture mechanics (Xie 1993 [20]), the stress intensity factor at the wing crack tip can be simplified into the superposition of the two stress intensity factors, as shown in Figs. 5(a) and 5(b).

$$K_I = K_I^{(1)} + K_I^{(2)} \,. \tag{6}$$

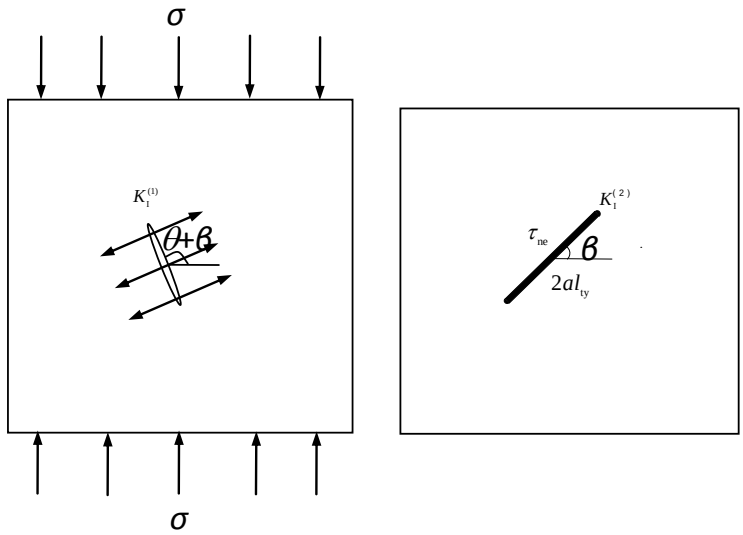

Fig. 5. Superposition of stress intensity factor of wing crack: (a) wing crack stress intensity factor $K_I^{(1)}$; (b) Equivalent of crack stress intensity factor $K_I^{(2)}$.

The two wing cracks at the two tips of the pre-existing crack are linked to form an isolation crack with a length of $2l$. Under the action of the axial compression σ, this isolation crack generates the stress intensity factor $K_I^{(1)}$. Simultaneously, the component $K_I^{(2)}$ is due to the effective shear stress induced by the axial compression. For the purpose of calculating $K_I^{(2)}$, the influence of the wing crack on the main crack is considered, and the influence coefficient l_{ty} is introduced. Then the pre-existing main crack can be calculated as $2al_{ty}$, the direction of which is the same as that one of the original crack.

In Eq. (6), $K_I^{(1)}$ is determined by the following equations:

$$\sigma_n' = \frac{1}{2}[\sigma + \sigma\cos 2(\theta+\beta)]\,, \tag{7}$$

$$K_I^{(1)} = -\sigma_n'\sqrt{\pi l} = -\frac{1}{2}[\sigma + \sigma\cos 2(\theta+\beta)]\sqrt{\pi l}\,. \tag{8}$$

The stress intensity factor of the equivalent straight crack, induced by the effective shear stress is given by (Baud et al 1996 [3]).

$$K_{II} = 2\tau_{ne}\sqrt{\frac{al_{ty}}{\pi}}\sin^{-1}\left(\frac{1}{l_{ty}}\right). \tag{9}$$

When the shear force reaches the critical value, the cracks begin to expand. Then, the tension wing crack forms at the tip of the main crack, and a certain angle θ emerges between wing crack surface and the original crack surface. Then, the stress intensity factor $K_I(\theta)$ produced by stress σ_θ in the direction of θ is (Baud et al. 1996 [3])

$$K_I(\theta) = \frac{3}{2} K_{II} \sin\theta \cos\frac{\theta}{2} . \tag{10}$$

Referring to Eq. (5), the equivalent stress intensity factor $K_I^{(2)}$ in the θ direction at the crack tip is calculated as

$$K_I^{(2)} = 3\tau_{ne}\sqrt{\frac{al_{ty}}{\pi}} \sin^{-1}\left(\frac{1}{l_{ty}}|big\right) \sin\theta \cos\frac{\theta}{2} . \tag{11}$$

Thus, the stress intensity factor K_I at the tip of the wing crack can be expressed as

$$K_I = 3\tau_{ne}\sqrt{\frac{al_{ty}}{\pi}} \sin^{-1}\left(\frac{1}{l_{ty}}\right) \sin\theta \cos\frac{\theta}{2} - \frac{1}{2}[\sigma + \sigma\cos 2(\theta+\beta)]\sqrt{\pi l} . \tag{12}$$

The influence coefficient l_{ty} is the function of the wing crack length l, the wing crack azimuth θ, and the main crack length a in the equation. Subsequently, the revised Horri and Nemat–Nasser wing crack model is introduced (Horri and Nemat1986 [9])

$$K_I = \frac{2a\tau_{ne}\sin\theta}{\sqrt{\pi(l+0.27a)}} - \sigma_n'\sqrt{\pi l} . \tag{13}$$

Comparing Eq. (12) with Eq. (13), we will get

$$3\tau_{ne}\sqrt{\frac{al_{ty}}{\pi}} \sin^{-1}(\frac{a}{al_{ty}}) \sin\theta \cos\frac{\theta}{2} = \frac{2a\tau_{ne}\sin\theta}{\sqrt{\pi(l+0.27a)}} . \tag{14}$$

As $l \to 0$, then we get

$$l_{ty} = \frac{0.667}{\cos^2(0.5\theta)} . \tag{15}$$

As $l \to \infty$, then we get

$$l_{ty} = 1 + \frac{9l\cos^2\dfrac{\theta}{2}}{4a} . \tag{16}$$

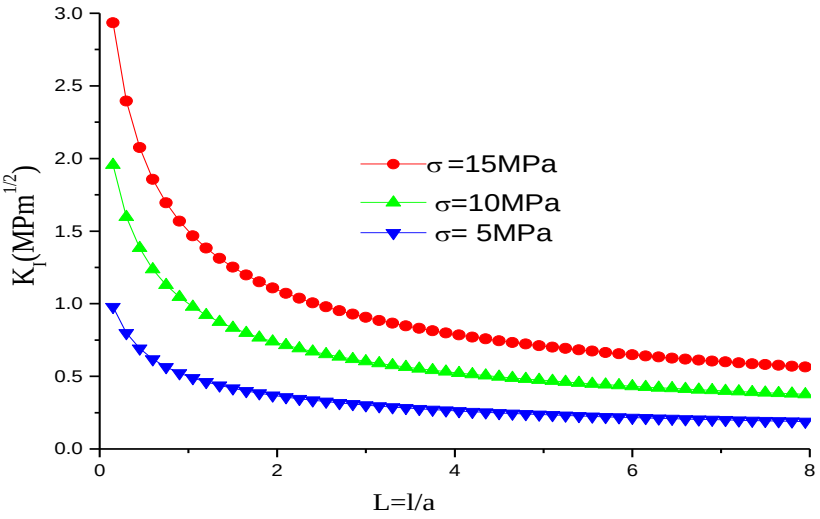

Fig. 6. Variation of K_I at the wing cracks tip with equivalent cracks propagation.

To meet the two conditions, the impact factor l_{ty} of the wing crack can be set as

$$l_{ty} = \left[1 + \frac{9l}{4a}\cos^2\left(\frac{\theta}{2}\right)\right](1 - e^{-l/a}) + 0.667\sec^2\left(\frac{\theta}{2}\right)e^{-l/a}\,. \tag{17}$$

The wing crack model is definite in physical meaning, and it can simulate the whole range of variation of wing crack length from extremely short to very long. Figure 6 shows the relationship between the stress intensity factor K_I at the crack tip and the equivalent crack propagation length L ($L = l/a$) under different axial compression. It is clear to see, that when axial compression is low, the wing crack expansion is stable. The stress intensity factor at the wing crack decrease with the equivalent crack length L. When $K_I < K_{IC}$ in Eq. (10), the wing crack will stop cracking. However, the stress intensity factor at the wing crack becomes greater with the increase of σ, the expansion of the wing crack becomes unstable under high axial compression.

In this experiment, it is found that the wing crack propagation failure model happened when the prefabricated crack angle is at a low value (25°). The wing cracks will expand approximately in the direction parallel to the maximum principal stress. For some specimens in this failure process, there are wing cracks appeared in both of the flaws, but which will not connect to each other until the failure of those specimens, as show in Fig. 7a. For some other specimens, there are wing cracks occurred only at one flaw, and the other flaw will keep stable until those specimens have damaged, as show in Fig. 7b. Further investigation revealed that this wing crack propagation

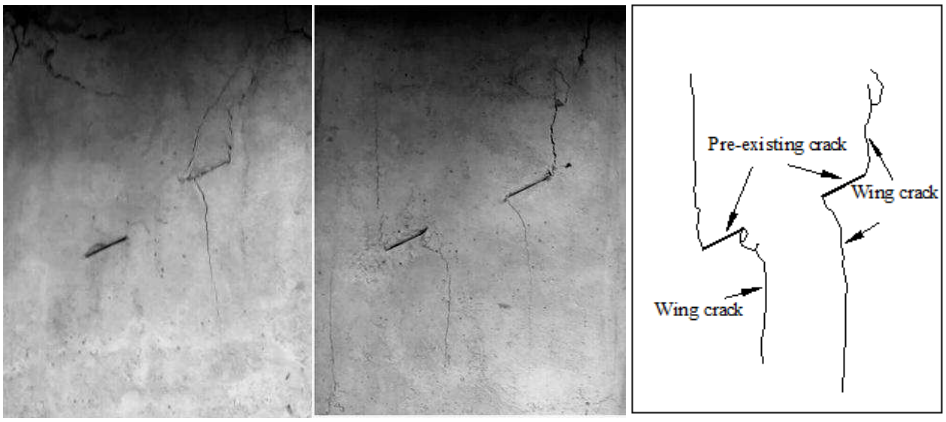

(a) (b)

Fig. 7. The wing crack propagation failure model.

failure model usually happened when the inclination angle of rock bridge is $\beta < 45°$, it is because when the inclination angle of rock bridge β at a low value, the effective shear stress on the crack is not big enough to develop shear cracks parallel to the main crack, but will produce wing cracks and driving its propagation. According to Eq. (12), when the wing crack extends to a critical length to the top of the specimen, the specimen begins to fail.

4. WING CRACK CONNECTION MODEL AND DAMAGE CRITERIA

As wing crack expands, the interaction of the cracks results in the continuous degradation of the macroscopic mechanical properties of the rock mass. Crack propagation, beginning with wing cracks, initiated along micro-cracks progressing to the complete damage of the rock mass, encompasses the evolution and accumulation of the rock mass damage, as well as the process of cracking the connection between cracks. By researching the characteristics of micro cracks formed at the crack tip, there are many failure modes divided (Steif 1984 [16]; Wong 1997 [18]; Pu 2010 [15]): wing crack propagation failure, wing cracks coalescence failure, wing crack connect to main crack failure, Secondary surface crack damage failure, wing crack connect to secondary surface crack failure, etc. In this experiment, according to the stress state along the failure crack surface, the gradual damage process of cracks generally has three forms (as show in Table 2): (1) the axial transfixion failure, (2) the tension-shear combined fracture failure, and (3) the wing crack shear connection failure. Based on the rock fracture mechanics criterion and the stress-strain curves during the failure process, the rock bridge cutting penetration damage mechanical

Table 2. The rock bridge fracture failure models under axial compression

Inclination angle of rock bridge [deg]	Inclination angle of rock bridge α [deg]	Failure models
$\beta = 25$	25	Wing crack propagation failure
	45	Tension-shear combined failure
	60	Tension-shear combined failure
	75	Tension-shear combined failure
	90	Axial transfixion failure
	105	Wing crack shear connection failure
$\beta = 45$	45	Tension-shear combined failure
	60	Tension-shear combined failure
	75	Tension-shear combined failure
	90	Axial transfixion failure
	105	Wing crack shear connection failure
$\beta = 60$	60	Tension-shear combined failure
	75	Wing crack shear connection failure
	90	Axial transfixion failure
	105	Wing crack shear connection failure
$\beta = 75$	75	Wing crack shear connection failure
	90	Axial transfixion failure
	105	Wing crack shear connection failure

models are established with different fracture transfixion failure modes under axial pressure.

4.1. THE AXIAL TRANSFIXION FAILURE

Whenever the wing crack extends stably or unstably, the tension wing crack connects the main crack in another row, as shown in Fig. 8. This kind of failure usually happened when the rock bridge approximately in the direction parallel to the maximum principal stress. When $\alpha = 90^{\circ}$, the rock bridge is right at the tensile stress path, driven by relative sliding fracture surface, which produces wing cracks at the crack tip. During the failure process, there are tension wing cracks appeared at both of the two main crack tips, then connected with the increase of the external loading. Although the rock bridge area failed during the wing crack propagation, there remains bearing capacity for the specimen, mainly withstood by the unbroken structure of the specimens, therefore its failure process is moderate.

For the stress and strain curves in this damage process, as show in Fig. 9, there are no obvious signs of damage failure to the specimen, when micro cracks appeared at

Fig. 8. The transfixion pattern of wing cracks under axial transfixion failure mode.

the crack tip. The specimen reaches its peak value when the stress and strain curves

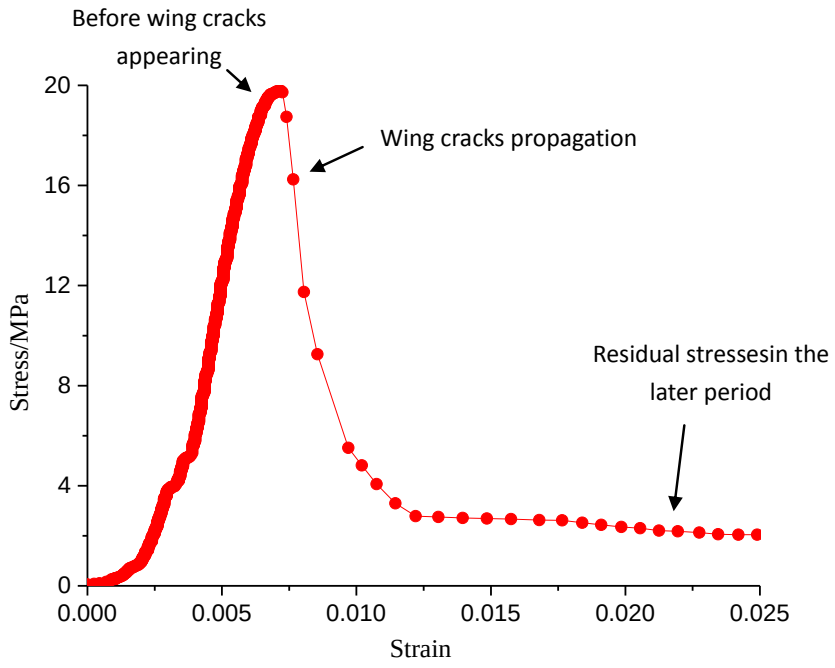

Fig. 9. The stress-strain curve under axial transfixion failure mode.

curved slightly, and the curve has an obvious decrease after the post-peak. Once the wing crack appears, it propagates fast along the direction of maximum compressive stress. In the later failure process, there is only small amount of granular material shall resist the load, so the residual strength of the specimen is low for this failure model.

For the axial transfixion failure, when the wing crack reaches the critical length $l_{1c} = b$ it happened wing crack propagation failure, and when $l_{1c} = b/2$ it happened wing crack connection failure. According to Eq. (12), taking the stress intensity at the crack tip as the criterion when the wing crack reaches the critical length, this paper establishes the failure criteria

$$K_I = 3\tau_{ne}\sqrt{\frac{al_{ty}}{\pi}}\sin^{-1}\left(\frac{1}{l_{ty}}\right)\sin\theta\cos\frac{\theta}{2} - \frac{1}{2}[\sigma + \sigma\cos 2(\theta+\beta)\sqrt{\pi l_{1c}}\,. \tag{18}$$

When $K_I(L_{IC}) \geq K_{IC}$, axial transfixion failure occurs in the rock bridge.

4.2. TENSION-SHEAR COMBINED FRACTURE FAILURE

This failure mode lies between the axial transfixion failure model and the wing crack shear connection failure model. As shown in Fig. 10, with the expansion of the wing crack under axial pressure, damage resistant capacity of the rock bridge is increasingly weakened. When the wing crack expands to a certain degree wing crack stops propagating on reaching some length, the rock bridge at the crack tip between the adjacent wing cracks fractured by the shear stress. Consequently, the crack is joined and connected in the shear direction, and shear damage occurs on the rock mass.

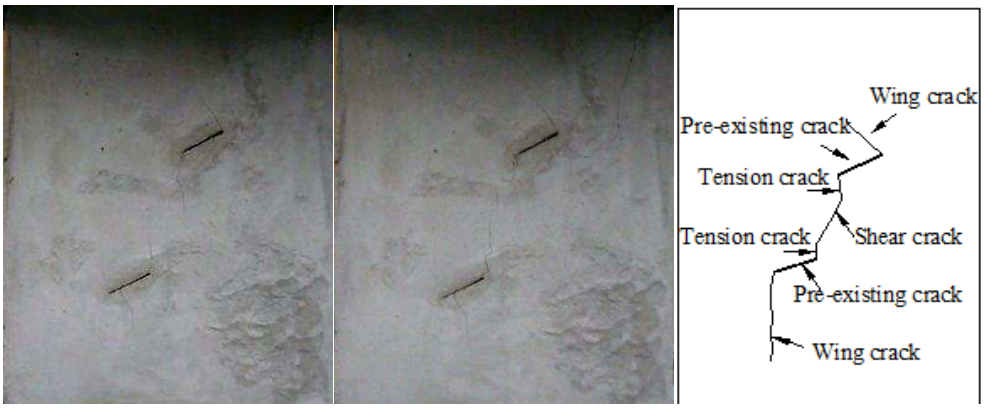

Fig. 10. The transfixion pattern of wing cracks under the tension-shear combined failure mode.

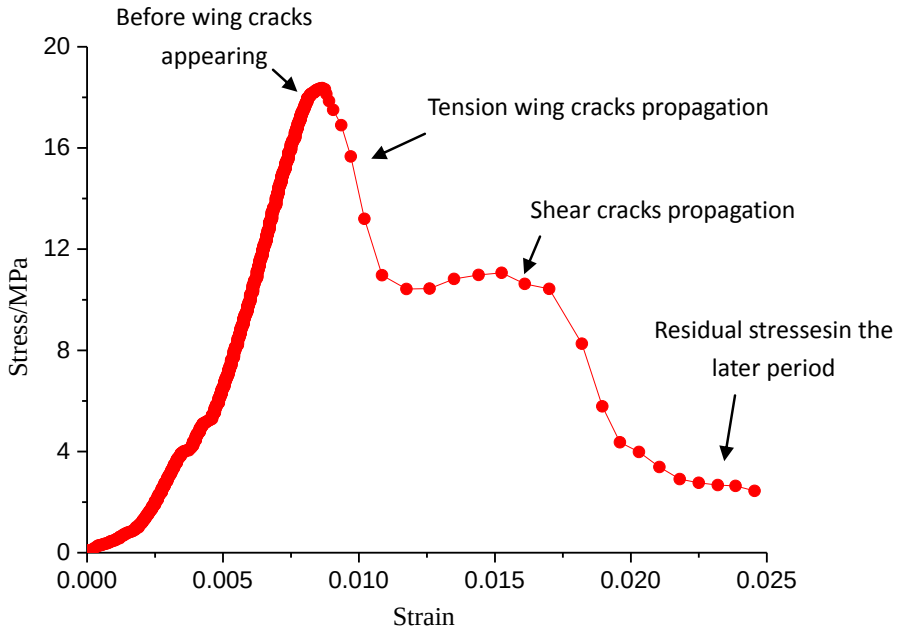

Fig. 11. The stress-strain curve under tension-shear combined failure mode.

For the stress and the strain curves in this damage process, as show in Fig. 11, the curve slope decreases obviously before wing crack initiating, it is because the wing crack appears relatively slower, that it did not cause larger relative sliding on the prefabricated crack surface, during its extension process. When the shear planes, produced by the shearing force begin to slide relatively, the particle body friction, playing the role of increasing resistance, makes this kind of specimen leaving with a larger residual stress. Such specimens have a good plastic deformation capacity as there is friction among the rock bridge.

Among these elements, as shown in Fig. 12, AB is 1/2 the length of the bottom crack, EF is 1/2 the length of the upper crack, CD is the rock bridge, BC and DE are the opened wing cracks, produced by the effective shear driving force of the main crack AB and EF, θ is the angle between rock bridge, and the maximum principal stresses σ_{CD} and τ_{CD} are the normal stress and shear stress, that acted on the rock bridge, respectively.

For the element shown in Fig. 12, we can obtain the mechanics balance as

$$\sum F_x = 0\,, \qquad \sum F_y = 0\,, \tag{19}$$

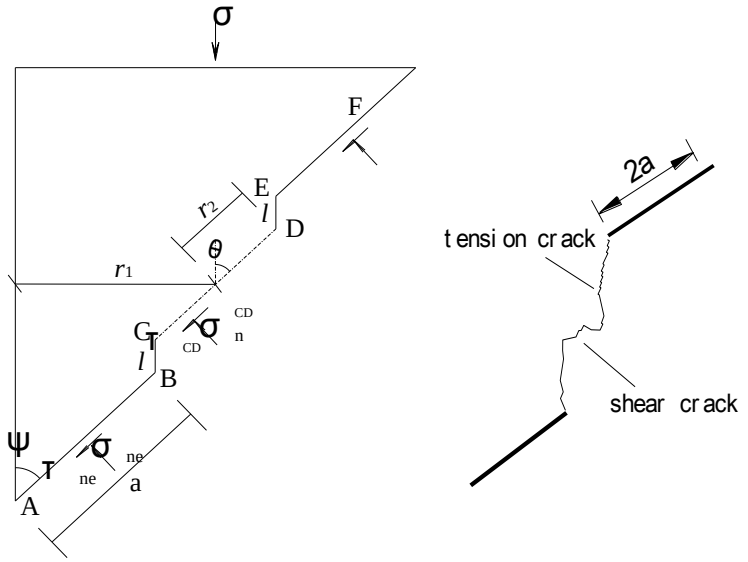

(a) (b)

Fig. 12. Tension-shear combined failure characteristics of rock bridge: (a) analysis of rock bridge stress; (b) rock bridge failure characteristics.

$$\begin{cases} 2a(\tau_{ne}\sin\psi+\sigma_{ne}\cos\psi)+2r_2(\tau_{CD}\sin\theta+\sigma_n^{CD}\cos\theta)=0\,, \\ 2r_1\sigma+2a(\tau_{ne}\cos\psi-\sigma_{ne}\sin\psi)+2r_2(\tau_{CD}\cos\theta-\sigma_n^{CD}\sin\theta)=0\,, \end{cases} \tag{20}$$

where

$$\begin{aligned} & r_1 a\sin\psi+\frac{1}{2}\sqrt{d^2+h^2}\,\sin\theta_0\,, \\ & r_2=\frac{\sqrt{d^2+h^2}\,\cos\theta_0-2l}{2\cos\theta}\,, \\ & \theta_0=\psi-\arcsin d/h \end{aligned} \tag{21}$$

Finally, we can obtain

$$\tau_{CD}=\frac{2A_2\tan\theta-2B_2}{(b\cos\theta_0-2l)(1+\tan^2\theta)}\,, \tag{22}$$

$$\sigma_{CD}=\frac{2A_2+2B_2\tan\theta}{(b\cos\theta_0-2l)(1+\tan^2\theta)}\,, \tag{23}$$

$$\begin{cases} A_2=-a(\tau_{ne}\sin\psi+\sigma_{ne}\cos\psi) \\ B_2=r_1\sigma+a(\tau_{ne}\cos\psi-\sigma_{ne}\sin\psi) \end{cases} \tag{24}$$

From Eqs (22) and (23), the strained condition of the rock bridge is relevant to rock bridge inclination θ, and the wing crack length l, etc. As the wing crack propagation length increases gradually, the shear strength between the rock bridge weakens continuously until the rock bridge connected completely, causing the destruction of the rock mass element. Assuming that the rock bridge shear damage meets the Mohr–Coulomb strength criterion, the conditions for the damage are:

$$\tau_{CD} - c - \sigma_{CD} \tan\varphi \geq 0\,. \tag{25}$$

Putting Eqs (22) and (23) into Eq. (25), the following is obtained:

$$\left(\frac{1}{2}b\cos\theta_0 - l\right)c\tan^2\theta + (B_2\tan\varphi - A_2)\tan\theta + A_2\tan\varphi + B_2 + \frac{1}{2}bc\cos\theta_0\,. \tag{26}$$

When the angle θ meets the rock bridge shear failure condition, the wing crack propagation length reaches a critical value l_{2c}. The angle θ between the rock bridge and σ_1 also reached critical values.

$$\theta_c = \arctan\frac{A_2 - B_2\tan\varphi + \sqrt{\Delta}}{\left(\sqrt{d^2+h^2}\,\cos\theta_0 - 2l_{2c}\right)c}\,. \tag{27}$$

From the geometric relations showed in Fig. 12

$$\tan\theta_c = \frac{b\sin\theta_0}{b\cos\theta_0 - 2l_{2c}}\,. \tag{28}$$

Combining Eq. (27) with Eq. (28), the critical length of the wing crack can be obtained.

$$l_{2c} = \frac{A_3 = \sqrt{A_3^2 - 4cB_3}}{2c}\,, \tag{29}$$

$$\begin{cases} A_3 = -a(tau_{nc}\sin\psi + \sigma_{ne}\cos\psi)\tan\varphi + B_2 + \frac{1}{2}b2c\cos\theta_0 \\ B_3 = \frac{1}{4}bc + \frac{1}{2}b\Big[(-a\tau_{ne}\sin\psi - a\sigma_{ne}\cos\psi)(\cos\theta_0\tan\varphi - \sin\theta_0) \\ \qquad\qquad +B_2(\sin\theta_0\tan\varphi + \cos\theta_0)\Big] \end{cases} \tag{30}$$

At the same time, according to Eq. (12), the stress intensity factor at the wing crack tip as the wing branch reaching the critical length is obtained.

$$K_I = 3\tau_{ne}\sqrt{\frac{al_{ty}}{\pi}}\sin^{-1}\left(\frac{1}{l_{ty}}\right)\sin\theta\cos\frac{\theta}{2} = \frac{1}{2}[\sigma + \sigma\cos 2(\theta+\beta)]\sqrt{\pi l_{2c}}\,. \tag{31}$$

4.3. WING CRACK SHEAR CONNECTION FAILURE

When the inclination angle of the rock bridge α is at a relative high value, wing crack shear connection failure model is the most common. Compared with the rock bridge tension damage, the wing crack emerges first. Then, it connects with another main crack to form a connected macro-fracture zone, as shown in Fig. 13.

For the stress and strain curves in this damage process, as show in Fig. 14, the curve is similar to that of the Tension-shear combined fracture failure model and due to the friction on the rough transfixion surface, making this kind of specimen has a larger residual stress. As shown in Fig. 15, BC is the wing cracks, CD is the rock bridge. The mechanics of the element are analyzed and combined with the balance equation to obtain

$$\begin{cases} -2a(\tau_{ne}\sin\psi + \sigma_{ne}\cos\psi) - r_3(\tau_{CD}\sin\theta + \sigma_n^{CD}\cos\theta) = 0\,, \\ 2r_1\sigma + 2a(\tau_{ne}\cos\psi - \sigma_{ne}\sin\psi) + r_3(\tau_{CD}\cos\theta - \sigma_n^{CD}\sin\theta) = 0\,, \end{cases} \tag{32}$$

where

$$r_3 = \frac{b\cos\theta_0 - l}{\cos\theta}\,. \tag{33}$$

Finally, we can obtain

$$\tau_{CD} = \frac{2A_4\tan\theta - 2B_2}{(b\cos\theta_0 - l)(1+\tan^2\theta)}\,, \tag{34}$$

(a) (b)

Fig. 13. The transfixion pattern of wing cracks under the wing crack shear connection failure mode.

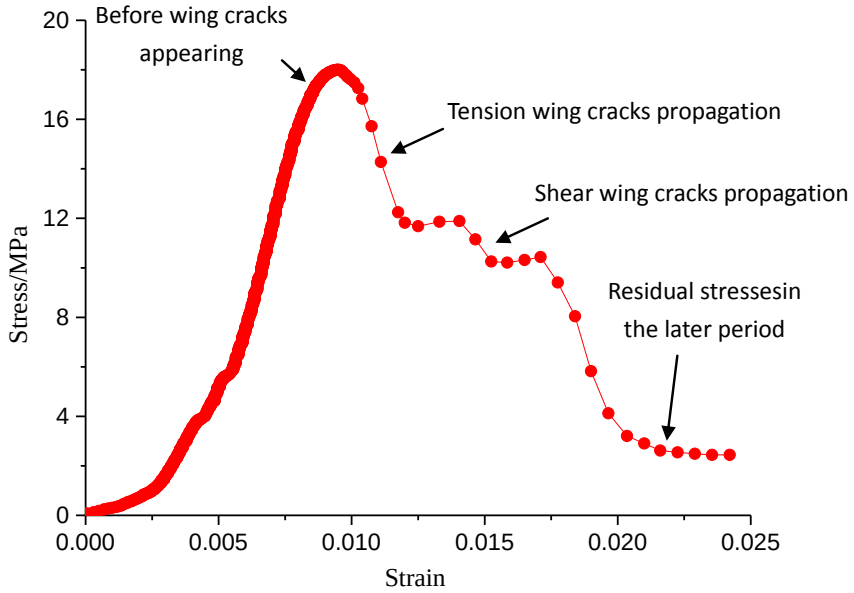

Fig. 14. The stress-strain curve under wing crack shear connection failure mode.

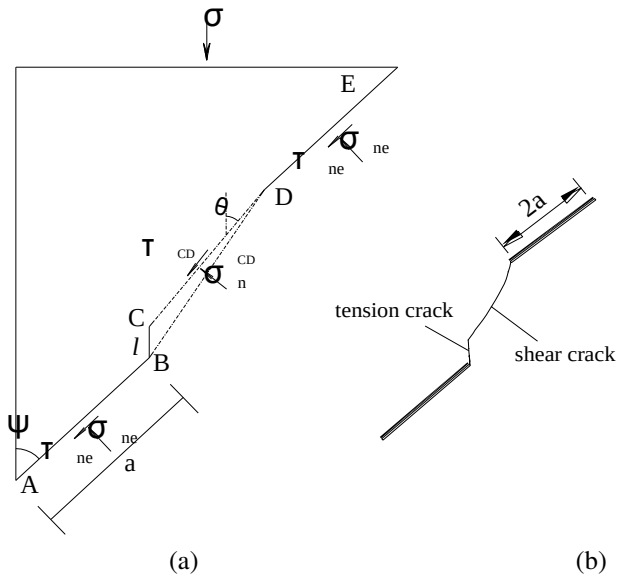

Fig. 15. Wing crack shear connection failure characteristics of rock bridge: (a) analysis of rock bridge stress; (b) rock bridge failure characteristics.

$$\sigma_{CD} = \frac{2A_4 + 2B_2 \tan\theta}{(b\cos\theta_0 - l)(1 + \tan^2\theta)}\,, \tag{35}$$

$$\begin{cases} A_4 = -a(\tau_{ne}\sin\psi + \sigma_{ne}\cos\psi) \\ B_2 = r_1\sigma + a(\tau_{ne}\cos\psi - \sigma_{ne}\sin\psi) \end{cases}. \tag{36}$$

Assuming, that the rock bridge shear damage meets the Mohr–Coulomb strength criterion, the conditions for the damage are:

$$\tau_{CD} - c - \sigma_{CD}\tan\varphi \geq 0\,. \tag{37}$$

Putting Eqs (34) and (35) into Eq. (37), the following is obtained:

$$\frac{1}{2}(b\cos\theta_0 - l)c\tan^2\theta + (B_2\tan\varphi - A_4)\tan\theta + A_4\tan\varphi + B_2 + \frac{1}{2}c(b\cos\theta_0 - l) \leq 0.$$

When angle θ meets the rock bridge shear failure condition, the wing crack propagation length reaches a critical value l_{3c}. The angle θ between the rock bridge and σ_1 also reached critical values.

$$\theta_c = \arctan\frac{A_4 - B_2\tan\varphi + \sqrt{\Delta}}{(b\cos\theta_0 - l_{3c})c}\,. \tag{38}$$

From the geometric relations shown in Fig. 15

$$\tan\theta_c = \frac{b\sin\theta_0}{b\cos\theta_0 - l_{3c}}\,. \tag{39}$$

Combining Eq. (38) with Eq. (39), the critical length of the wing crack can be obtained.

$$l_{3c} = \frac{A_5 = \sqrt{A_5^2 - 4B_3c}}{2c}\,, \tag{40}$$

$$\begin{cases} A_5 = -a(tau_{nc}\sin\psi + \sigma_{ne}\cos\psi)\tan\varphi + B_2 + bc\cos\theta_0 \\ B_3 = \frac{1}{4}bc + \frac{1}{2}b\Big[a(-\tau_{ne}\sin\psi - \sigma_{ne}\cos\psi)(\cos\theta_0\tan\varphi - \sin\theta_0) \\ \qquad\qquad +B_2(\sin\theta_0\tan\varphi + \cos\theta_0)\Big] \end{cases}, . \tag{41}$$

At the same time, according to Eq. (12), the stress intensity factor at the crack tip when the wing crack reaches the critical length is obtained.

$$K_I = 3\tau_{ne}\sqrt{\frac{al_{ty}}{\pi}}\sin^{-1}\left(\frac{1}{l_{ty}}\right)\sin\theta\cos\frac{\theta}{2} = \frac{1}{2}[\sigma + \sigma\cos 2(\theta + \beta)]\sqrt{\pi l_{3c}}\,. \tag{42}$$

To sum up, the strength criterion for the fracture damage occurring on the fractured rock mass under uniaxial compression is established. When the rock bridge fractured, the critical length of the wing crack is not only relevant to the rock features and the far field stress, but it is also influenced by the geometric location of the crack.

5. CONCLUSIONS

The compression test on rock-like specimens with two pre-existing transfixion fissures, made by pulling out the embedded metal inserts in the pre-cured period, was carried out on the servo control uniaxial loading tester. The failure evolution mechanism of the rock sample was analysed, combined with the stress-strain curves when axial transfixion failure, tension-shear combined failure, or wing crack shear connection failure occurs on the rock bridge under axial compression. The cracking phenomena and the crack patterns observed experimentally have served as valuable references for the theoretical work. The results are as follows:

(1) It was found that under uniaxial compression, according to the different geometry of pre-existing cracks, the specimen with two precast crack will occur wing crack failure or rock bridge fracturing failure. The determinant for different failure modes is the effective shear driving relative sliding on the surface. When fracture specimens with prefabricated crack occurs coalesce failure, according to the failure mechanism of the rock bridge, axial transfixion failure, wing crack shear connection failure, and tension-shear combined failure are classified.

(2) Inclination angle of the rock bridge is the main factor influencing the characteristics of the rock bridge: the specimen is given priority to axial transfixion failure when the inclination angle of rock bridge nearly parallel to the direction of maximum principal stress, given priority to wing crack shear connection failure, when the inclination angle of rock bridge α is at a relative high value, and given priority to tension-shear combined failure in the transition state. Basing on the rock fracture mechanics, the rock bridge's cutting penetration damage mechanical models of the compression shear rock mass are established for three different fracture transfixion failure modes.

(3) For the intact specimens, the strength curve has an significant decrease, after the post-peak and leaving with a low residual strength, it has the mechanics characteristic of brittle material. Comparing to the stress-strain curves of intact specimens, as a result of the existence of friction enhancement effect on the transfixion failure surface, the prefabricated crack specimen with different failure models will not completely lose its bearing capacity in an instant after the peak strength, it has the mechanics characteristic of elastic-plastic material. The results obtained were of significance in studying the failure mechanism of fractured rock mass.

ACKNOWLEDGMENT

This paper gets its funding from Project (51174228, 51274249, 51304240, 51474249) supported by National Natural Science Foundation of China; The authors wish to acknowledge these supports.

REFERENCES

[1] ASHBY, M. F., S. D. HALLAM. The Failure of Brittle Solids Containing Small Cracks under Compressive Stress States. *Acta Metall.*, **34** (1986), No. **3**, 497-510.

[2] ASHBY, M. F., C. G. SAMMIS. The Damage Mechanics of Brittle Solids in Compression. *Pure Appl. Geophys.*, **133** (1990), No. **3**, 489-521.

[3] BAUD, P, T. REUSCHLE, P. CHARLEZ. An improved Wing Crack Model for the Deformation and Failure of Rock in Compression. *Int. J. Rock Mech. Min. Sci.*, **33** (1996), No. **5**, 539-542.

[4] BOBET, A. Fracture Coalescence in Rock Materials: Experimental Observations and Numerical Predictions, MIT, Massachusetts, Cambridge, 1997.

[5] CAO, P., T. LIU, C. Z. PU ET AL. Crack Propagation and Coalescence of Brittle Rock-like Specimens with Pre-existing Cracks in Compression. *Engineering Geology*, **187** (2015), 113-121.

[6] CAO, P., C. Z. PU. Failure Characteristics and its Influencing Factors of Rock-like Material with Multi-fissures under Uniaxial Compression. *Transactions of Nonferrous Metals Society of China*, **22** (2012), No. **1**, 185-191.

[7] DYSKIN, A. V., E. SAHOURYEH, R. J. JEWELL. Influence of Shape and Locations of Initial 3-D Cracks on Their Growth in Uniaxial Compression. *Engineering Fracture Mechanics*, **70** (2003), 2115-2136.

[8] HOEK, E., C. D. MARTIN. Fracture Initiation and Propagation in Intact Rock – A Review. *Journal of Rock Mechanics and Geotechnical Engineering*, **6** (2014), No. **4**, 287-300.

[9] HORII, H., S. NEMAT. Brittle Failure in Compression: Splitting, Faulting and Brittle-ductile Transition. *J. Phil. Trans. R. Soc. London A*, **139** (1986), 337-374.

[10] KEMENY, J. M., N. G. W. COOK. Crack Models for the Failure of Rocks in Compression, In: Constitutive Laws for Engineering Materials: Theory and Applications, Amsterdam, Elsevier, 1987, 879-887.

[11] KEMENY, J. M. A Model for Nonlinear Rock Deformation under Compression due to Subcritical Crack Growth. *Int. J. Rock Mech. Min. Sci.,* **28** (1991), 459-467.

[12] LAJTAI, E. Z. Microscopic Fracture Processes in a Granite. *Rock Mech. Rock Eng.,* **31** (1998), No. **4**, 237-250.

[13] LI, S. Z. W. Fracture Damage Mechanism of Discontinuous jinted Rokmass under the State of Complex Stress and its Application. *Chinese Journal of Rock Mechanics and Engineering,* **18** (1999), No. **2**, 142-146.

[14] PARK, C. H., A. BOBET. Crack Initiation, Propagation and Coalescence from Frictional Flaws in Uniaxial Compression. *Engineering Fracture Mechanics,* **77** (2010), 2727-2748.

[15] PU, C. Z. Experiment Research on the Fracture Failure Mechanism of Rock-like Material with Fissures under Uniaxial Vompression, Changsha, Central South University, 2010, 37-50.

[16] STEIF, P. S. Crack Extension under Compressive Loading. *Eng. Fract. Mech.*, **20** (1984), 463-473.

[17] TANG, C. A., S. Q. KOU. Crack Propagation and Coalescence in Brittle Materials under Compression. *Engineering Fracture Mechanics*, **61** (1998), No. **3**, 311-324.

[18] WONG, R. H. C. Failure Mechanisms, Peak Strength of Natural Rocks and Rock-like Solids Containing Frictional Cracks, Hong Kong, The Hong Kong Polytechnic University, 1997, 123-142.

[19] WONG, L. N. Y., H. H. EINSTEIN. Crack Coalescence in Molded Gypsum and Carrara Marble – Part 1. Macroscopic Observations and Interpretation. *Rock Mech. Rock Eng.*, **42** (2009), No. **3**, 475-511.

[20] XIE, H. Fractals in Rock Mechanics, Netherlands, A. A. Balkema Publishers, 1993.

[21] YANG, S. Q., D. S. YANG, H. W. JING. An Experimental Study of the Fracture Coalescence Behaviour of Brittle Sandstone Specimens Containing Three Fissures. *Rock Mech. Rock Eng.*, **45** (2012), 563-582.

[22] ZHANG, X. P., L. N. Y. WONG. Crack Initiation, Propagation and Coalescence in Rock-Like Material Containing Two Flaws: A Numerical Study Based on Bonded-Particle Model Approach. *Rock Mech. Rock Eng.,* **46** (2013), No. **5**, 1001-1021.

[23] ZHENG, S. H. Research on Coupling Theory between Seepage and Damage of Fractured Rock Mass and its Application to Engineering, Wuhan Institute of Rock and Soil Mechanics, Chinese Academy of Scinces, 2000, 95-102.

[24] ZHOU, X. P., Y. X. ZHANG, Q. L. HA. Micromechanical Modelling of the Complete Stress-Strain Relationship for Crack Weakened Rock Subjected to Compressive Loading. *Rock Mech. Rock Eng.*, **41** (2008), No. **5**, 747-769.